11. V. I. Prokhorenko *et al.*, *Science* **313**, 1257 (2006).
12. J. Savolainen *et al.*, *Proc. Natl. Acad. Sci. U.S.A.* **105**, 7641 (2008).
13. I. Otake, S. S. Kano, A. Wada, *J. Chem. Phys.* **124**, 014501 (2006).
14. C. Daniel *et al.*, *Science* **299**, 536 (2003).
15. M. P. A. Branderhorst *et al.*, *Science* **320**, 638 (2008).
16. R. A. Bartels, M. M. Murnane, H. C. Kapteyn, I. Christov, H. Rabitz, *Phys. Rev. A* **70**, 043404 (2004).
17. D. Cardoza, C. Trallero-Herrero, F. Langhojer, H. Rabitz, T. Weinacht, *J. Chem. Phys.* **122**, 124306 (2005).
18. M. A. Montgomery, R. R. Meglen, N. H. Damrauer, *J. Phys. Chem. A* **110**, 6391 (2006).
19. M. A. Montgomery, R. R. Meglen, N. H. Damrauer, *J. Phys. Chem. A* **111**, 5126 (2007).
20. J. L. White, B. J. Pearson, P. H. Bucksbaum, *J. Phys. At. Mol. Opt. Phys.* **37**, L399 (2004).
21. $2G_2$-m-Per is a second-generation dendrimer with two monodendrons on meta positions and an ethynylene perylene trap.
22. Z. H. Peng, J. S. Melinger, V. Kleiman, *Photosynth. Res.* **87**, 115 (2006).
23. E. Atas, Z. H. Peng, V. D. Kleiman, *J. Phys. Chem. B* **109**, 13553 (2005).
24. Z. H. Peng, Y. C. Pan, B. B. Xu, J. H. Zhang, *J. Am. Chem. Soc.* **122**, 6619 (2000).
25. Materials and methods are available as supporting material on *Science* Online.
26. S. F. Swallen, R. Kopelman, J. S. Moore, C. Devadoss, *J. Mol. Struct.* **486**, 585 (1999).
27. D. Meshulach, Y. Silberberg, *Nature* **396**, 239 (1998).
28. D. Meshulach, D. Yelin, Y. Silberberg, *Opt. Commun.* **138**, 345 (1997).
29. T. Brixner, N. H. Damrauer, B. Kiefer, G. Gerber, *J. Chem. Phys.* **118**, 3692 (2003).
30. M. H. B. Schmidt, G. Stobrawa, T. Feurer, LAB2-A virtual femtosecond laser lab, www.lab2.de.
31. L. G. C. Rego, L. F. Santos, V. S. Batista, *Annu. Rev. Phys. Chem.* **60**, 293 (2009).
32. D. Meshulach, Y. Silberberg, *Phys. Rev. A* **60**, 1287 (1999).
33. M. A. Montgomery, N. H. Damrauer, *J. Phys. Chem. A* **111**, 1426 (2007).
34. V. D. Kleiman, S. M. Arrivo, J. S. Melinger, E. J. Heilweil, *Chem. Phys.* **233**, 207 (1998).
35. T. Brixner, N. H. Damrauer, P. Niklaus, G. Gerber, *Nature* **414**, 57 (2001).
36. J. P. Ogilvie, K. J. Kubarych, A. Alexandrou, M. Joffre, *Opt. Lett.* **30**, 911 (2005).

37. This work was supported by the NSF, CHE-0239120.

Supporting Online Material
www.sciencemag.org/cgi/content/full/326/5950/263/DC1
Materials and Methods
SOM Text
Figs. S1 to S11
References

19 May 2009; accepted 31 August 2009
10.1126/science.1176524

Repetitive Readout of a Single Electronic Spin via Quantum Logic with Nuclear Spin Ancillae

L. Jiang,[1]*† J. S. Hodges,[1,2]* J. R. Maze,[1]* P. Maurer,[1] J. M. Taylor,[3]‡ D. G. Cory,[2] P. R. Hemmer,[4] R. L. Walsworth,[1,5] A. Yacoby,[1] A. S. Zibrov,[1] M. D. Lukin[1]§

Robust measurement of single quantum bits plays a key role in the realization of quantum computation and communication as well as in quantum metrology and sensing. We have implemented a method for the improved readout of single electronic spin qubits in solid-state systems. The method makes use of quantum logic operations on a system consisting of a single electronic spin and several proximal nuclear spin ancillae in order to repetitively readout the state of the electronic spin. Using coherent manipulation of a single nitrogen vacancy center in room-temperature diamond, full quantum control of an electronic-nuclear system consisting of up to three spins was achieved. We took advantage of a single nuclear-spin memory in order to obtain a 10-fold enhancement in the signal amplitude of the electronic spin readout. We also present a two-level, concatenated procedure to improve the readout by use of a pair of nuclear spin ancillae, an important step toward the realization of robust quantum information processors using electronic- and nuclear-spin qubits. Our technique can be used to improve the sensitivity and speed of spin-based nanoscale diamond magnetometers.

Efforts have recently been directed toward the manipulation of several qubits in quantum systems, ranging from isolated atoms and ions to solid-state quantum bits (*1*, *2*). These small-scale quantum systems have been successfully used for proof-of-concept demonstrations of simple quantum algorithms (*3*–*6*). In addition, they can be used for potentially important practical applications in areas such as quantum metrology (*1*). For example, techniques involving quantum logic operations on several trapped ions have been applied to develop an improved ion state readout scheme, resulting in a new class of atomic clocks (*7*, *8*). We developed a similar technique to enhance the readout of a single electronic spin in the solid state.

Our method makes use of quantum logic between a single electronic spin and nuclear spin qubits in its local environment for repetitive readout. Although such nuclear spins are generally the source of unwanted decoherence in the solid state, recent theoretical (*9*–*11*) and experimental (*12*–*18*) work has demonstrated that when properly controlled, the nuclear environment can become a very useful resource, in particular for long-term quantum memory.

Our experimental demonstration makes use of a single negatively charged nitrogen-vacancy (NV) center in diamond. The electronic ground state of this defect is an electronic spin triplet (with spin $S = 1$) and is a good candidate for a logic qubit on account of its remarkably long coherence times (*19*) and fast spin manipulation by use of microwave fields (*20*). Furthermore, the center can be optically spin-polarized and measured by combining confocal microscopy techniques with spin-selective rates of fluorescence (*12*). In practice, the NV spin readout under ambient room-temperature conditions is far from perfect. This is because laser radiation at 532 nm for readout repolarizes the electronic spin before a sufficient number of photons can be scattered for the state to be reliably determined.

Our approach is to correlate the electronic-spin logic qubit with nearby nuclear spins (*21*), which are relatively unperturbed by the optical readout, before the measurement process (*22*). Specifically, we used one or more ^{13}C nuclei (with nuclear spin $I = 1/2$) nuclear spins in the diamond lattice, coupled to the NV electronic spin via a hyperfine interaction, as memory ancillae qubits. For example, a single ^{13}C nuclear spin has eigenstates $|\uparrow\rangle_{n1}$ (aligned) or $|\downarrow\rangle_{n1}$ (anti-aligned) with the local magnetic field. The composite electronic-nuclear system was first prepared in a fiducial state, $|0\rangle_e\,|\downarrow\rangle_{n1}$, by using a sequence of optical, microwave, and radiofrequency (RF) pulses. Next, the electronic spin was prepared in an arbitrary state $|\Psi\rangle_e = \alpha|0\rangle_e + \beta|1\rangle_e$, where $|0,1\rangle_e$ denote electronic state with projected spin momentum m_S (m_S) = 0, 1. Before readout, we performed a sequence of gate operations resulting in the entangled electron-nuclear state $|\Psi\rangle_e\,|\downarrow\rangle_{n1} \rightarrow \alpha|0\rangle_e\,|\downarrow\rangle_{n1} + \beta|1\rangle_e\,|\uparrow\rangle_{n1}$. The optical measurement process projects this state into either $|0\rangle_e\,|\downarrow\rangle_{n1}$ or $|1\rangle_e\,|\uparrow\rangle_{n1}$. When optically excited, these two states fluoresce at different rates dependent on the value of m_S. Within a typical measurement period, less than one photon was counted before the electron spin was repolarized to $|0\rangle_e$, which indicates that the uncertainty of the electronic spin-state measurement is quite large.

The nuclear spin can thus reveal the former electronic state because of the correlations established before the electronic spin was reset. To achieve this repetitive readout, we performed a controlled-not operation, which mapped $|0\rangle_e\,|\downarrow\rangle_{n1} \rightarrow |0\rangle_e\,|\downarrow\rangle_{n1}$ and $|0\rangle_e\,|\uparrow\rangle_{n1} \rightarrow |1\rangle_e\,|\uparrow\rangle_{n1}$, and repeated the

---

[1] Department of Physics, Harvard University, Cambridge, MA 02138, USA. [2] Department of Nuclear Science and Engineering, Massachusetts Institute of Technology (MIT), Cambridge, MA 02139, USA. [3] Department of Physics, MIT, Cambridge, MA 02139, USA. [4] Department of Electrical and Computer Engineering, Texas A&M University, College Station, TX 77843, USA. [5] Harvard-Smithsonian Center for Astrophysics, Cambridge, MA 02138, USA.

*These authors contributed equally to this work.
†Present address: Institute for Quantum Information, California Institute of Technology, Pasadena, CA 91125, USA.
‡Present address: Joint Quantum Institute, University of Maryland, College Park, MD 20742, USA.
§To whom correspondence should be addressed. E-mail: lukin@fas.harvard.edu

Downloaded from on February 26, 2016

optical measurement. Fluorescence counting of these two states can be added to prior measurements so as to decrease the uncertainty for electronic spin-state discrimination. If optical readout does not destroy the orientation of the nuclear spin, the uncertainty in the determination of the electronic spin can be reduced via repetitive measurements. In this way, the overall signal-to-noise of the measurement process of our logic qubit can be increased. After multiple readout cycles and many quantum logic operations, the nuclear spin orientation will finally be destroyed. However, it is possible to further improve the readout scheme by using a pair of ancillary nuclear spins and imprinting the electronic state into a Greenberger-Horne-Zeilinger (GHZ)–like state: $|\Psi\rangle_e |\downarrow\rangle_{n1} |\downarrow\rangle_{n2} \rightarrow \alpha|0\rangle_e |\downarrow\rangle_{n1} |\downarrow\rangle_{n2} + \beta|1\rangle_e |\uparrow\rangle_{n1} |\uparrow\rangle_{n2}$. In such a case, the state of the first nuclear spin after repetitive readout sequences can be periodically "refreshed" by using the information stored within the second nuclear spin. These schemes are closely related to a quantum nondemolition (QND) measurement (*23*, *24*) because the nuclear spin-population operators $\hat{I}_z^{n1,n2}$ do not evolve throughout the electronic-spin readout and constitute "good" QND observables. Although imperfect, optical NV electronic spin detection precludes an ideal QND measurement, our scheme nevertheless allows substantial improvement in the spin readout.

To implement the repetitive readout technique, we used a single NV center in diamond coupled to nearby ^{13}C nuclear spins. These nuclear spins can be polarized and fully controlled and provide a robust quantum memory, even in the presence of optical radiation necessary for electronic spin-state readout (*13*, *22*). This is achieved through a combination of optical, microwave, and RF fields (Fig. 1) and is discussed in (*25*).

To control a single nuclear spin, we chose a NV center with a well-resolved ^{13}C hyperfine coupling near 14 MHz. The degeneracy of the $|m_S = \pm1\rangle_e$ spin states was lifted by applying a $B_0 = 30$ gauss magnetic field along the NV axis. Under these conditions, the transitions of the electronic spin (**e**) within the subspace of $\{|0\rangle_e, |1\rangle_e\}$ can be selectively addressed, conditioned on a certain nuclear state. The model Hamiltonian for this system (Fig. 1A) is

$$H = (\Delta + \gamma_e B_0)\hat{\mathcal{S}}_z + \gamma_C B_0 \hat{I}_z^{n1} + A\hat{\mathcal{S}}_z\hat{I}_z^{n1} \qquad (1)$$

where $\Delta = 2\pi \times 2.87$ GHz is the zero field splitting, A is the hyperfine interaction, and γ_e and γ_C are the electronic- and nuclear-spin gyromagnetic ratios. $\hat{\mathcal{S}}_z = \frac{1}{2}\hat{\mathbf{1}} + \hat{S}_z$ is a pseudo-spin one-half operator for the electronic spin subspace, $\hat{\mathbf{1}}$ is the identity matrix, and $\hat{I}_z^{n1}$ and $\hat{S}_z$ are the spin-1/2 angular momentum operators. Coherent oscillations between the $|0\rangle_e$ and $|1\rangle_e$ states, conditioned on a single proximal nuclear spin ($\mathbf{n}_1$) in $|\downarrow\rangle_{n1}$ (or $|\uparrow\rangle_{n1}$), were selectively driven by the microwave field MW1 (or MW2). To control nuclear spin $\mathbf{n}_1$, a resonantly tuned RF field to address the levels $|1\rangle_e |\downarrow\rangle_{n1}$ and $|1\rangle_e |\uparrow\rangle_{n1}$, which are energetically separated because of the hyperfine interaction (Fig. 1A), was used. After the initialization of spin **e**, spin $\mathbf{n}_1$ was polarized by applying MW1 and RF π pulses, which transfers the polarization from spin **e** to spin $\mathbf{n}_1$. Rabi oscillations of spin $\mathbf{n}_1$ were demonstrated (Fig. 1E) by preparing spin **e** in the $|1\rangle_e$ state irrespective of the state of spin $\mathbf{n}_1$ (by using MW1 and MW2 π-pulses) and increasing the RF pulse length. These data indicate that we can achieve spin $\mathbf{n}_1$ preparation (polarization) and readout with combined fidelity $F \equiv \langle\downarrow| \rho' |\downarrow\rangle \geq 75\%$, where ρ' is the reduced density operator for spin $\mathbf{n}_1$.

We now describe the repetitive readout technique. As illustrated in Fig. 1D, the direct readout of electronic spin is imperfect. We define n^0 and n^1 as the total number of photons detected for the $|0\rangle_e$ and $|1\rangle_e$ states, respectively, during a single measurement interval. The signal is defined as the difference in average counts between the two spin states: $A_0 = n^0 - n^1 \approx 0.005$ (Fig. 1D). Experimentally, photon shot-noise dominated the fluctuations in the counts. Because of this shot

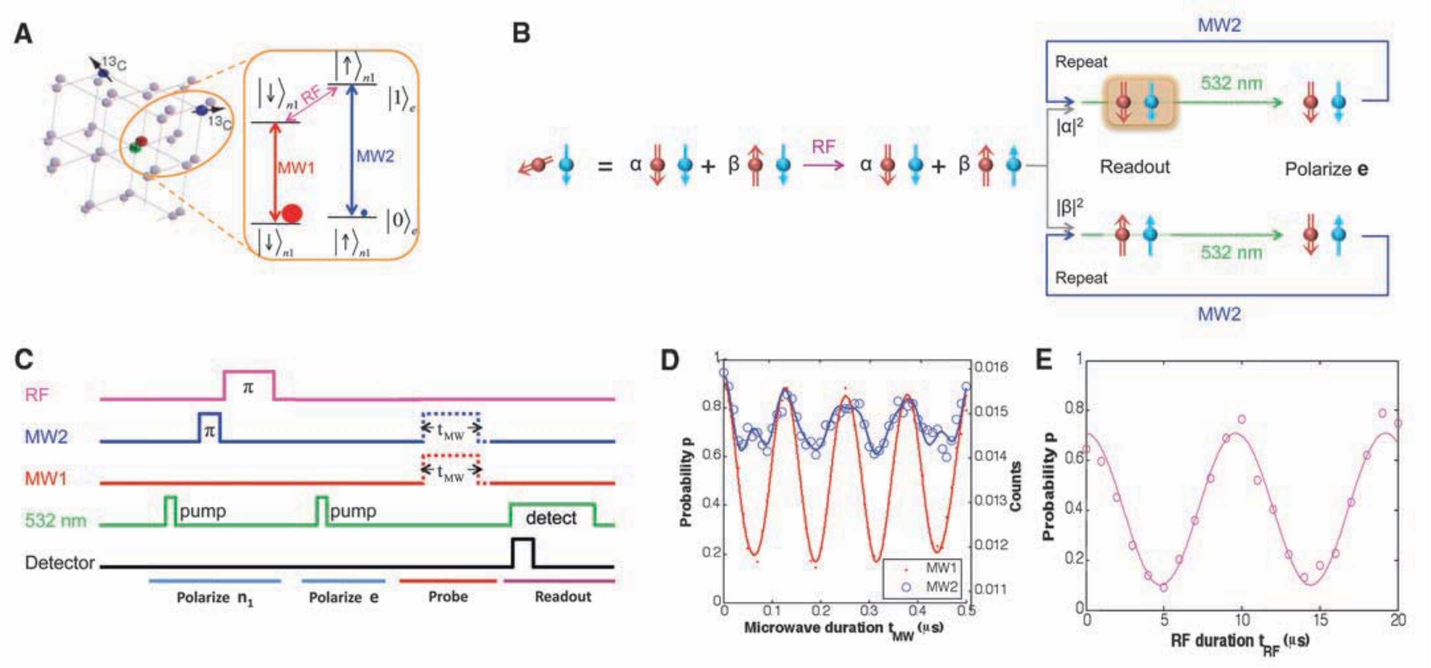

Fig. 1. Repetitive readout of an electronic spin. (**A**) Illustration of the NV center and its proximal ^{13}C nuclear spins. (Inset) Energy levels of the coupled spin system formed by the NV electronic spin (**e**) and the first proximal ^{13}C nuclear spin ($\mathbf{n}_1$). With a static magnetic field applied along the NV axis, spin $\mathbf{n}_1$ keeps the same quantization axis when spin **e** is $|0\rangle_e$ or $|1\rangle_e$ (*25*). When spin $\mathbf{n}_1$ is $|\downarrow\rangle_{n1}$ (or $|\uparrow\rangle_{n1}$), the microwave field MW1 (or MW2) resonantly drives spin **e** between $|0\rangle_e$ and $|1\rangle_e$, which can implement the $C_{n1}NOT_e$ gate. When spin **e** is $|1\rangle_e$, the RF field resonantly drives spin $\mathbf{n}_1$ between $|\downarrow\rangle_{n1}$ and $|\uparrow\rangle_{n1}$, which can implement the C_eNOT_{n1} gate. (**B**) Illustration of repetitive readout. The red down arrow represents the electronic spin state $|0\rangle_e$, the red up arrow represents the electronic spin state $|1\rangle_e$, the blue down arrow represents the nuclear spin state $|\downarrow\rangle_{n1}$, and the blue up arrow represents the nuclear spin state $|\uparrow\rangle_{n1}$. (**C**) Experimental pulse sequences that polarize spin $\mathbf{n}_1$ to $|\downarrow\rangle_{n1}$ and spin **e** to $|0\rangle_e$, followed by various probe operations, before fluorescence readout of spin **e**. (**D**) Measured electronic spin Rabi oscillations driven by MW1 and MW2 fields for polarized spin $\mathbf{n}_1$. The small wiggles for MW2 are due to off-resonant driving of the majority population in the $|\downarrow\rangle_{n1}$ state. The data are in agreement for finite detunings and microwave power (solid curves). The right vertical axis shows the average counts for a single readout. The left vertical axis shows the probability in the $|0\rangle_e$ state, obtained from the average counts (*25*). (**E**) Measured nuclear spin Rabi oscillation driven by the RF field.

noise and the low average count ($n^0 \approx 0.016$), we needed to average over $N \sim 10^5$ experimental runs in order to obtain the data in Fig. 1D.

To improve the signal, we used two spins: **e** and $\mathbf{n}_1$. Both spins were first polarized to the initial state $|0\rangle_e\,|\downarrow\rangle_{n1}$. Next, we performed a unitary operation $U(t)$, which prepares the superposition state $|\Psi_1\rangle = (\alpha|0\rangle_e + \beta|1\rangle_e)\,|\downarrow\rangle_{n1}$ that we wanted to measure. Instead of immediately reading out the electronic spin, we use a controlled-not gate ($C_e\mathrm{NOT}_{n1}$, achieved with an RF π pulse) to correlate spin **e** with spin $\mathbf{n}_1$ (Fig. 2A). We then optically readout/pumped spin **e**, leaving the spin system in the post-readout state: $\rho_{\mathrm{post}} = |0\rangle\langle 0|_e \otimes (|\alpha|^2\,|\downarrow\rangle\langle\downarrow| + |\beta|^2\,|\uparrow\rangle\langle\uparrow|)_{n1}$. The state of spin $\mathbf{n}_1$ via the electronic spin **e** by performing a controlled-not operation ($C_{n1}\mathrm{NOT}_e$, achieved with an MW1 or MW2 π pulse) was then readout. This completes a one-step readout of spin $\mathbf{n}_1$, which can be repeated.

As a direct illustration of the enhanced readout technique, Fig. 2C shows the accumulated signal for Rabi oscillations of the electronic spin obtained by adding M subsequent repetitive readouts for each experimental run. This procedure results in a 10-fold enhancement of spin signal amplitude.

In order to further quantify the performance of this technique, the noise added with each additional repetitive readout must be considered. The repetitive readout spin signal is defined as a weighted sum of difference counts A_m associated with mth readout: $S_w(M) = \sum_{m=1}^{M} w_m A_m$. The average values of A_m were determined experimentally by measuring the difference in average counts associated with Rabi oscillations for each mth repeated readout. The w_m allowed us to weight the contribution of each repetitive readout to the overall signal. The noise corresponding to the repetitive readout signal is $\Delta S_w(M) = \sqrt{\sum_{m=1}^{M} w_m^2 \sigma_m^2}$. Here, σ_m is the uncertainty of the measurement of A_m. Experimentally, this uncertainty was found to be independent of m.

The signal-to-noise figure of merit is defined as $SNR\,(M) = S_w(M)/\Delta S_w(M)$. The w_m weights were chosen by noting that the larger values of A_m allow us to extract more information given the fixed uncertainty of each measurement, and we should emphasize these readouts more. As proven in (*25*), the optimal choice of weights corresponds to $w_m = |A_m|/\sigma_m^2$, and the optimized SNR is given by

$$\mathrm{SNR}_{opt}(M) = \sqrt{\sum_{m=1}^{M} \left|\frac{A_m}{\sigma_m}\right|^2} \qquad (2)$$

In the ideal QND case, each repetitive readout would yield the same $|A_m|$, and the SNR would scale with $\sqrt{M}$. For our experiment, the SNR saturates (Fig. 2E) because of the decay of the normalized amplitudes (Fig. 3D). Nevertheless, the experimental data shown in Fig. 2E indicate the enhancement of SNR by more than 220%.

In assessing this result, it is noted that various imperfections can affect the repetitive readout, which leads to the imperfect first readout $|A_1|/|A_0| < 1$, the sharp decrease in $|A_2|$, and the subsequent exponential reduction $|A_m| = |A_2|\eta^{(m-2)}$, with $\eta \approx 0.95$. These behaviors can be attributed to three major imperfections (*25*): (i) errors from microwave pulses (about 7% error probability for each π pulse), (ii) imperfect optical pumping of the electronic spin after each readout; and most substantially (iii) the depolarization of the nuclear-spin memory under optical illumination.

To quantify the latter process, we studied the decay times for ^{13}C nuclear spins in the presence of optical illumination. For an illumination time t_L longer than 1 μs, the nuclear spin polarization decays exponentially, with a characteristic time of τ_{n1} = 13 (1) μs (Fig. 3B). Because τ_{n1} is much longer than the time for optical readout and optical spin polarization of the NV electronic spin (350 ns), repetitive readout of **e** is possible. [In the absence of optical illumination, the ^{13}C nuclear spin decay times are >>1 ms (*12*, *13*).] Despite the relatively long τ_{n1}, after many cycles the nuclear spin depolarizes. This degrades the repetitive optical readout for larger m, yielding the overall exponential decay in the amplitude $|A_m|$ with increasing m (*25*).

As an indication of how this limit can be circumvented, the use of two ancillary nuclear spins

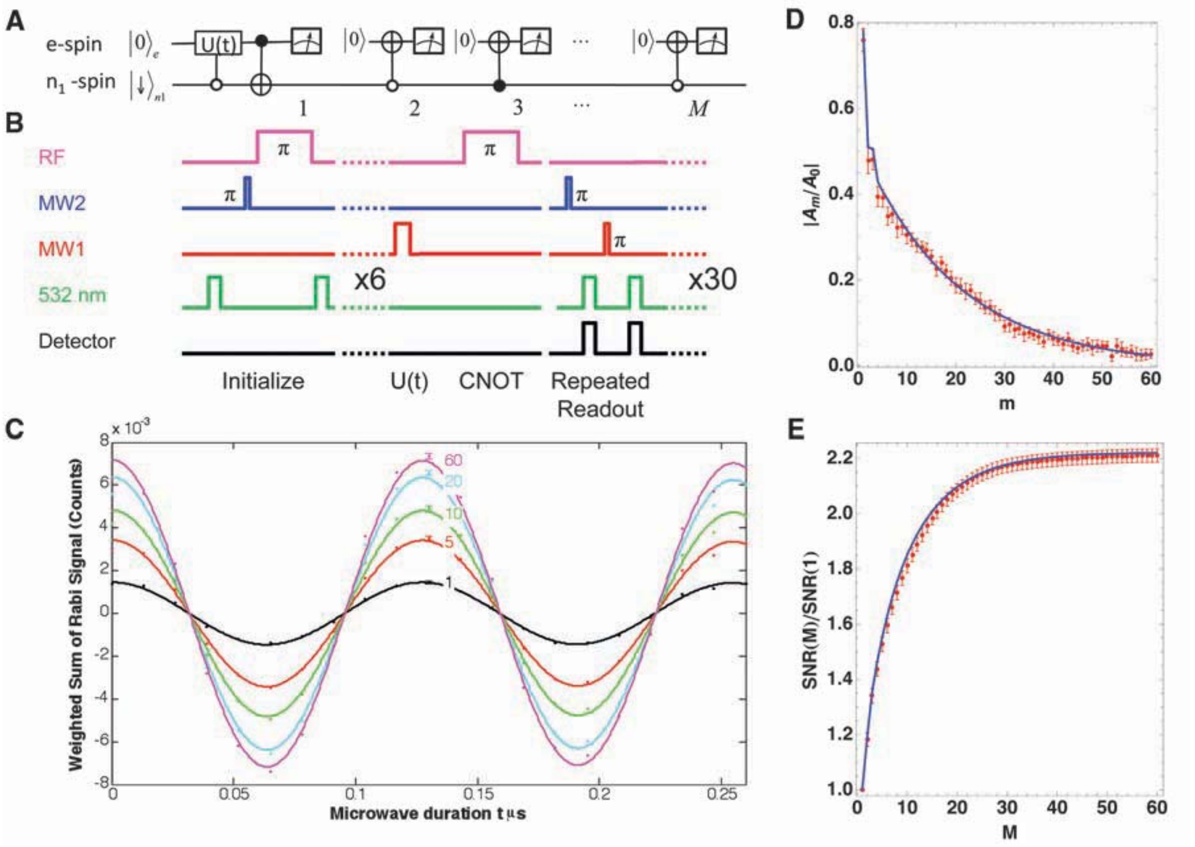

Fig. 2. Realization of repetitive readout. (**A**) Quantum circuit for M-step repetitive readout scheme assisted by spin $\mathbf{n}_1$. (**B**) Operations and pulse sequences for $M = 60$. The initial state $|0\rangle_e\;|\downarrow\rangle_{n1}$ is prepared with a six-step pumping of spins **e** and $\mathbf{n}_1$. The MW1 pulse of duration t induces the Rabi rotation $U(t)$ of spin **e**, whose parity information is imprinted to spin $\mathbf{n}_1$ with an RF π pulse (the $C_e\mathrm{NOT}_{n1}$ gate). After fluorescence readout of spin **e**, (M − 1)–repetitive readouts of spin $\mathbf{n}_1$ are performed by means of MW1 or MW2 π pulses ($C_{n1}\mathrm{NOT}_e$ gates) followed by fluorescence readout. The m = 1 readout is not preceded by a MW1 pulse. (**C**) Cumulative signal obtained from repetitive readout measurements, summed from m = 1 to M, for M = 1, 5, 10, 20, and 60 repetitions. Constant background counts are subtracted. (**D**) Amplitudes $|A_m|$ for Rabi oscillation measurements obtained from the mth readout normalized to the signal amplitude without repetitive readout (A_0). (**E**) Improvement in SNR using the repetitive readout scheme. Blue curves in (D) and (E) are simulations with imperfection parameters estimated from independent experiments (*25*).

was considered. The state of spin **e** may be correlated with a more distant spin $\mathbf{n}_2$ in addition to proximal spin $\mathbf{n}_1$. As the decay time of spin $\mathbf{n}_2$ is longer than that of spin $\mathbf{n}_1$ because of a weaker interaction with spin **e**, the information stored in spin $\mathbf{n}_2$ persists after spin $\mathbf{n}_1$ has been depolarized under optical illumination. This remaining $\mathbf{n}_2$ polarization can then be transferred to spin $\mathbf{n}_1$ and repetitively readout again.

Control of two nuclear spins is achieved by using the strongly coupled nuclear spin $\mathbf{n}_1$ as a probe for the second nearby ^{13}C nuclear spin $\mathbf{n}_2$, which cannot be directly observed via the NV center. By placing the NV electronic spin in $|0\rangle_e$ state, the hyperfine coupling is removed. This enables proximal ^{13}C nuclear spins with similar Zeeman energy to flip-flop and exchange spin population. Figure 3D shows that the nuclear population, $p_{n1,\uparrow}(\tau)$, oscillates between $p_{n1,\uparrow}(0) \approx 0.2$ and $p_{n1,\uparrow}(T/2) \approx 0.5$ with a period of $T = 117$ (1) μs (Fig. 3, A and C). The relatively high contrast of these oscillations suggests an interaction with a second nuclear spin ($\mathbf{n}_2$) as the two nuclei flip-flop between the states $|\uparrow\rangle_{n1}\,|\downarrow\rangle_{n2}$ and $|\downarrow\rangle_{n1}\,|\uparrow\rangle_{n2}$. Such an excitation exchange requires a similar Zeeman splitting for the two spins, indicating that the second nucleus is also a ^{13}C. The nuclear spin-spin interaction strength determined by our measurements, $b = \pi/T = 4.27$ (3) kHz, is several times that of a bare dipolar coupling (2 kHz for two ^{13}C nuclei separated by the nearest neighbor distance, 1.54 Å), signifying that their interaction is mediated by the NV electronic spin (Fig. 3A, inset) (*25*), which is described by the interaction hamiltonian $H_{\text{int}} = b(I_{1+}I_{2-} + I_{1-}I_{2+})$. This interaction can be used to effectively control the state of the second nucleus and of the entire three-spin system. Specifically, a half period of nuclear spin oscillation, $T/2$, constitutes a SWAP (*1*) operation between the two nuclear spins. This operation can be used, for example, to polarize the second nuclear spin (Fig. 3, C and D). In addition, by modifying the initial state of spin $\mathbf{n}_1$, we can prepare the initial state of the two nuclei in any of the four possible configurations: ↑↑, ↑↓, ↓↑, or ↓↓ (*25*). Further control is provided by putting the electronic spin into the $|1\rangle_e$ state, in which case the flip-flop dynamics between spins $\mathbf{n}_1$ and $\mathbf{n}_2$ disappears (fig. S1). This is because spins $\mathbf{n}_1$ and $\mathbf{n}_2$ typically have very distinct hyperfine splittings that introduce a large energy difference ($\Delta E >> b$) between $|\uparrow\rangle_{n1}\,|\downarrow\rangle_{n2}$ and $|\downarrow\rangle_{n1}\,|\uparrow\rangle_{n2}$ and quench the interaction. Therefore, we can implement a controlled-SWAP operation between spins $\mathbf{n}_1$ and $\mathbf{n}_2$, enabling full control over spin $\mathbf{n}_2$. We further observed that spin $\mathbf{n}_2$ has a decay time of $\tau_{n2} = 53$ (1) μs (Fig. 3B, inset) under

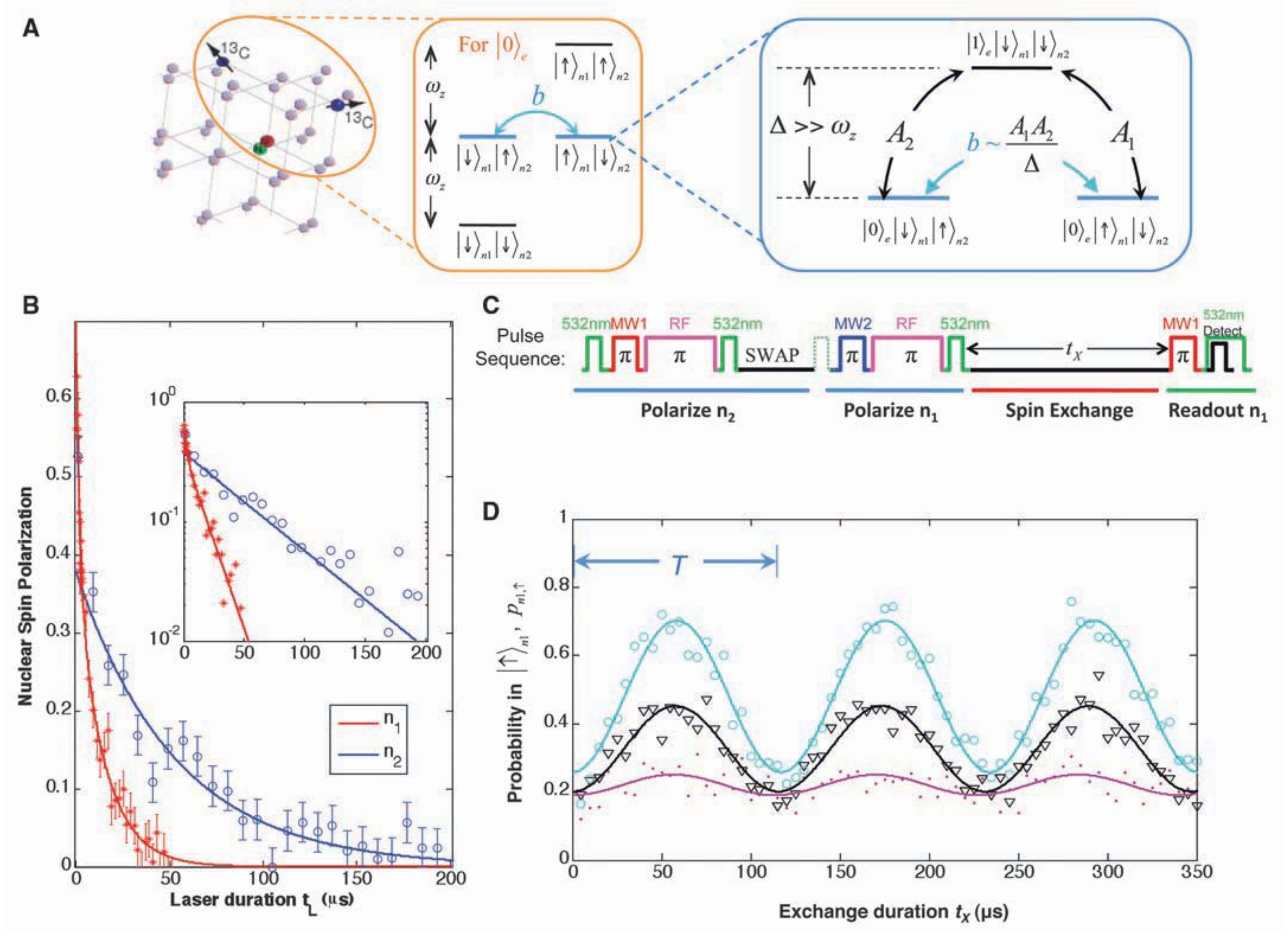

Fig. 3. Coherence and control of two nuclear spins. (**A**) The coupled spin system formed by the NV electronic spin (**e**) and two proximal ^{13}C nuclear spins ($\mathbf{n}_1$ and $\mathbf{n}_2$). (Middle) Energy levels for spins $\mathbf{n}_1$ and $\mathbf{n}_2$ when spin **e** is in the $|0\rangle_e$ state. (Right) Schematic of flip-flop between spins $\mathbf{n}_1$ and $\mathbf{n}_2$, which is electron-mediated by the second-order hopping via $|1\rangle_e\,|\downarrow\rangle_{n1}\,|\downarrow\rangle_{n2}$. (**B**) Measured depolarization of spins $\mathbf{n}_1$ and $\mathbf{n}_2$ under optical illumination. For the duration of optical illumination t_L longer than 1 μs, the polarizations for spins $\mathbf{n}_1$ and $\mathbf{n}_2$ decay exponentially with characteristic times $\tau_{n1} = 13$ (1) μs and $\tau_{n2} = 53$ (5) μs, respectively. For t_L less than 1 μs, the decay is slightly faster, which is probably associated with dynamics of the spin-fluctuator model that describe optically induced depolarization of single nuclei (*22*, *25*). These decay times are much longer than the optical readout/pump time of the electronic spin (about 350 ns). (Inset) Log-linear plot. (**C**) Operations and pulse sequence to probe dynamics between spins $\mathbf{n}_1$ and $\mathbf{n}_2$. (**D**) Measured spin flip-flop dynamics between spins $\mathbf{n}_1$ and $\mathbf{n}_2$. For three different preparations of the initial state [$|\downarrow\rangle_{n1}\,|\uparrow\rangle_{n2}$ (blue), $|\downarrow\rangle_{n1}$ and n_2 in thermal state (black), and $|\downarrow\rangle_{n1}\,|\downarrow\rangle_{n2}$ (purple)], the observed population, $p_{n1,\uparrow}(t)$, oscillates with the same period $T = 117$ (1) μs. These observations verify the theoretical prediction, with flip-flop coupling strength $b = 4.27$ (3) kHz.

optical illumination. Compared with spin $\mathbf{n}_1$, spin $\mathbf{n}_2$ is less perturbed by the optical transitions between different electronic states because it has a weaker hyperfine coupling to the electron (*22*).

To demonstrate concatenated readout experimentally, both nuclear spins were initialized in the state $|\downarrow\rangle_{n1}\,|\downarrow\rangle_{n2}$, and a single NV electronic spin that we would like to detect was prepared in a superposition state $(\alpha|0\rangle + \beta|1\rangle)_e$. First, the operation ($C_e\mathrm{NOT}_{n1}$-SWAP-$C_e\mathrm{NOT}_{n1}$) was used to prepare the GHZ-type state $|\Psi\rangle = \alpha|0\rangle_e\,|\downarrow\rangle_{n1}\,|\downarrow\rangle_{n2} + \beta|1\rangle_e\,|\uparrow\rangle_{n1}\,|\uparrow\rangle_{n2}$. Next, we optically readout/pumped spin **e**, leaving the system in state $\rho'_{\mathrm{post}} = |\alpha|^2\,|0\downarrow\downarrow\rangle\langle 0\downarrow\downarrow| + |\beta|^2\,|0\uparrow\uparrow\rangle\langle 0\uparrow\uparrow|$. $M - 1$ repetitive readouts of spin $\mathbf{n}_1$ were then performed in the manner described above until spin $\mathbf{n}_1$ was depolarized. At that point, spin $\mathbf{n}_2$ was still directly correlated with the first measurement of the **e** spin. This information can be transferred to spin $\mathbf{n}_1$ by means of a nuclear SWAP gate. Thus, the parity information can be measured again by performing a second round of M-step repetitive readout. These operations are summarized in the quantum circuit (Fig. 4A) and pulse sequences (Fig. 4B).

Experimentally, the "revival" in the signal amplitude $|A_m|$ after the SWAP was demonstrated (Fig. 4C), which led to an associated jump in the SNR curve (Fig. 4D) for $M' = 61$. This shows that the second nuclear spin can be used to further enhance the readout efficiency. Although ideally the repetitive readout scheme assisted by two nuclear spins should improve the absolute SNR more than a single nuclear spin, in the present experimental realization this is not yet so because more errors are accumulated for the two-nuclear-spin scheme because of initialization and pulse imperfections. These errors reduce the optical signal amplitudes for the readout assisted by two nuclear spins, compromising the overall SNR improvement. Nevertheless, the experiments clearly demonstrate that it is in principle possible to further boost the relative SNR by using additional nuclear spins.

Although we have demonstrated an enhancement for coherent Rabi oscillations, any set of pulses acting on the electronic spin (such as a spin echo sequence) can be implemented. This should have immediate applications to NV-based nanomagnetometry (*26*, *27*). Because the duration of the entire repetitive readout sequence (~150 μs in Fig. 2B) is shorter than the typical echo duration in pure diamond, SNR improvements directly translate into enhanced sensitivity and increased speed of nanoscale diamond magnetometer (*28*). This may have important applications in probing time-varying processes in biophysical systems. The repetitive readout can also be used to achieve single-shot readout of NV centers. At room temperature, with optimized collection efficiency, an improvement in spin signal on the order of a few hundred is needed to achieve single-shot readout. Potentially, this improvement can be obtained by using nuclei more robust to optical depolarization, such as the nitrogen nuclear spin of the NV center in isotopically pure ^{12}C diamond (*19*) and by using advanced control techniques (*29*, *30*) to suppress the imperfections from microwave pulses. Furthermore, resonant optical excitations [wavelength $\lambda \approx 637$ nm] can be used for NV centers at cryogenic temperatures. Here, the resolved spin structure of optical excited states (*20*, *31*, *32*) can be exploited to readout the electronic spin much more efficiently with reduced perturbation to the nuclear spin (*22*). Under these conditions, a 10-fold spin signal improvement may be sufficient to enable single-shot readout of the NV electronic spin. In turn, this can be used to perform robust, adaptive QND measurements of nuclear-spin qubits, which will be of direct use for distributed quantum networks (*13*, *21*). Our experiments demonstrate that manipulation of several nuclear-spin ancillae surrounding a central electronic spin can be used to implement useful quantum algorithms in solid-state systems.

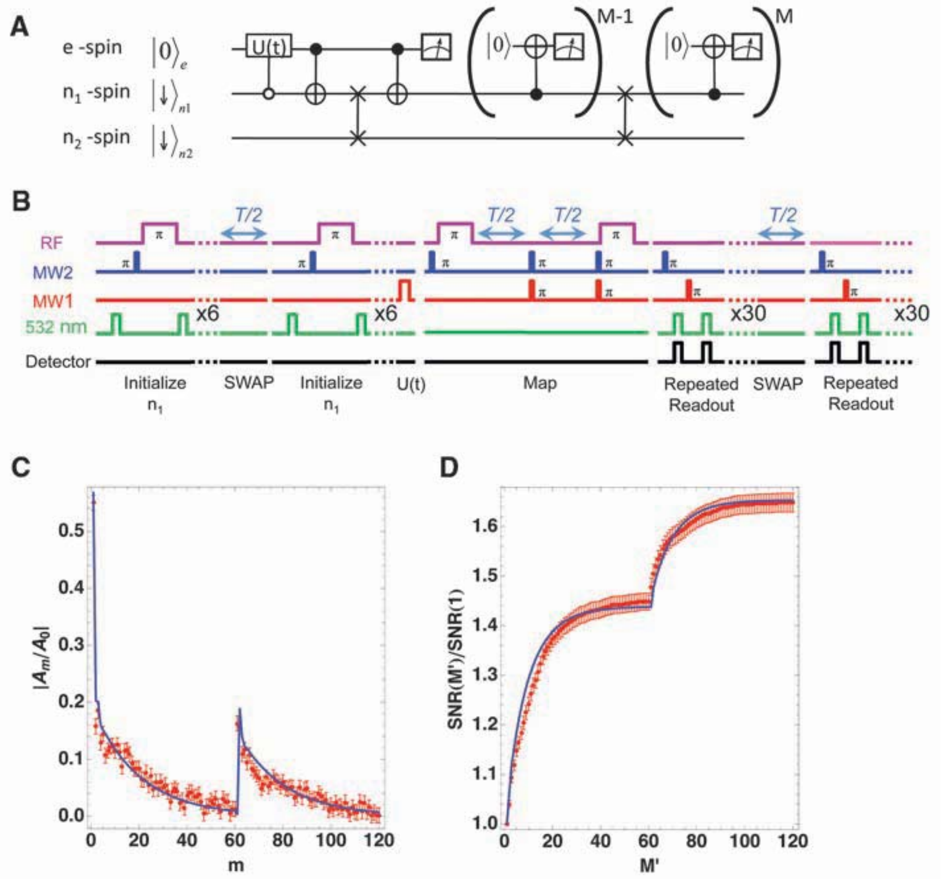

Fig. 4. Demonstration of the two-level concatenated readout procedure. (**A**) Quantum circuit for concatenated M-step repetitive readout scheme assisted by both spins $\mathbf{n}_1$ and $\mathbf{n}_2$. (**B**) Operations and pulse sequences for $M = 60$. Ideally, the GHZ-like state $\alpha|0\rangle_e\,|\downarrow\rangle_{n1}\,|\downarrow\rangle_{n2} + \beta|1\rangle_e\,|\uparrow\rangle_{n1}\,|\uparrow\rangle_{n2}$ with the parity information of spin **e** imprinted on both spins $\mathbf{n}_1$ and $\mathbf{n}_2$ is created before the first readout. After the first round of M-step repetitive readout, spin $\mathbf{n}_1$ is depolarized, but spin $\mathbf{n}_2$ maintains its polarization. The spin state of spin $\mathbf{n}_2$ is swapped to spin $\mathbf{n}_1$, which is then detected during the second round of M-step repetitive readouts. (**C**) Normalized amplitude $|A_m|/|A_0|$ obtained from the mth readout. (**D**) Measured improvement in the SNR by use of the double repetitive readout scheme. The blue curves in (C) and (D) are simulations with imperfection parameters estimated from independent experiments (*25*).

References and Notes

1. R. Blatt, D. Wineland, *Nature* **453**, 1008 (2008).
2. R. Hanson, D. D. Awschalom, *Nature* **453**, 1043 (2008).
3. M. Riebe *et al.*, *Nature* **429**, 734 (2004).
4. R. Reichle *et al.*, *Nature* **443**, 838 (2006).
5. L. DiCarlo *et al.*, *Nature* **460**, 240 (2009).
6. C. A. Ryan, C. Negrevergne, M. Laforest, E. Knill, R. Laflamme, *Phys. Rev. A* **78**, 012328 (2008).
7. T. Rosenband *et al.*, *Science* **319**, 1808 (2008).
8. D. B. Hume, T. Rosenband, D. J. Wineland, *Phys. Rev. Lett.* **99**, 120502 (2007).
9. W. M. Witzel, S. Das Sarma, *Phys. Rev. B* **77**, 165319 (2008).
10. J. Maze, J. M. Taylor, M. D. Lukin, *Phys. Rev. B* **78**, 094303 (2008).
11. W. A. Coish, J. Fischer, D. Loss, *Phys. Rev. B* **77**, 125329 (2008).
12. F. Jelezko *et al.*, *Phys. Rev. Lett.* **93**, 130501 (2004).
13. M. V. G. Dutt *et al.*, *Science* **316**, 1312 (2007).
14. P. Neumann *et al.*, *Science* **320**, 1326 (2008).
15. R. Hanson, V. V. Dobrovitski, A. E. Feiguin, O. Gywat, D. D. Awschalom, *Science* **320**, 352 (2008).
16. J. J. L. Morton *et al.*, *Nat. Phys.* **2**, 40 (2006).
17. J. S. Hodges, J. C. Yang, C. Ramanathan, D. G. Cory, *Phys. Rev. A* **78**, 010303 (2008).
18. J. J. L. Morton *et al.*, *Nature* **455**, 1085 (2008).
19. G. Balasubramanian *et al.*, *Nat. Mater.* **8**, 383 (2009).
20. G. D. Fuchs *et al.*, *Phys. Rev. Lett.* **101**, 117601 (2008).
21. L. Jiang, J. M. Taylor, A. S. Sorensen, M. D. Lukin, *Phys. Rev. A* **76**, 062323 (2007).
22. L. Jiang *et al.*, *Phys. Rev. Lett.* **100**, 073001 (2008).
23. S. Haroche, J. M. Raimond, *Exploring the Quantum: Atoms, Cavities, and Photons* (Oxford Univ. Press, New York, 2006).
24. M. Sarovar, K. C. Young, T. Schenkel, K. B. Whaley, *Phys. Rev. B* **78**, 245302 (2008).
25. Materials and methods are available as supporting material on *Science* Online.

26. J. R. Maze *et al.*, *Nature* **455**, 644 (2008).
27. G. Balasubramanian *et al.*, *Nature* **455**, 648 (2008).
28. J. M. Taylor *et al.*, *Nat. Phys.* **4**, 810 (2008).
29. N. Khaneja, T. Reiss, C. Kehlet, T. Schulte-Herbruggen, S. J. Glaser, *J. Magn. Reson.* **172**, 296 (2005).
30. P. Cappellaro, L. Jiang, J. S. Hodges, M. D. Lukin, *Phys. Rev. Lett.* **102**, 210502 (2009).
31. N. B. Manson, J. P. Harrison, M. J. Sellars, *Phys. Rev. B* **74**, 104303 (2006).
32. A. Batalov *et al.*, *Phys. Rev. Lett.* **102**, 195506 (2009).

33. We thank P. Cappellaro, L. Childress, J. Doyle, M. V. G. Dutt, J. MacArthur, A. Sorenson, P. Stanwix, E. Togan, and A. Trifonov for many stimulating discussions and experimental help. This work was supported by the Defense Advanced Research Projects Agency, NSF, the Packard Foundation, and the Pappalardo Fellowship. The content of the information does not necessarily reflect the position or the policy of the U.S. Government, and no official endorsement should be inferred.

Supporting Online Material
www.sciencemag.org/cgi/content/full/1176496/DC1
Materials and Methods
Figs. S1 to S4
References

19 May 2009; accepted 29 July 2009
Published online 10 September 2009;
10.1126/science.1176496
Include this information when citing this paper.

Persistent Currents in Normal Metal Rings

A. C. Bleszynski-Jayich,[1] W. E. Shanks,[1] B. Peaudecerf,[1] E. Ginossar,[1] F. von Oppen,[2] L. Glazman,[1,3] J. G. E. Harris[1,3]

Quantum mechanics predicts that the equilibrium state of a resistive metal ring will contain a dissipationless current. This persistent current has been the focus of considerable theoretical and experimental work, but its basic properties remain a topic of controversy. The main experimental challenges in studying persistent currents have been the small signals they produce and their exceptional sensitivity to their environment. We have developed a technique for detecting persistent currents that allows us to measure the persistent current in metal rings over a wide range of temperatures, ring sizes, and magnetic fields. Measurements of both a single ring and arrays of rings agree well with calculations based on a model of non-interacting electrons.

An electrical current induced in a resistive circuit will rapidly decay in the absence of an applied voltage. This decay reflects the tendency of the circuit's electrons to dissipate energy and relax to their ground state. However, quantum mechanics predicts that the electrons' many-body ground state (and, at finite temperature, their thermal equilibrium state) may contain a persistent current (PC), which flows through the resistive circuit without dissipating energy or decaying. A dissipationless equilibrium current flowing through a resistive circuit is counterintuitive, but it has a familiar analog in atomic physics: Some atomic species' electronic ground states possess nonzero orbital angular momentum, which is equivalent to a current circulating around the atom.

One of the major insights of mesoscopic condensed-matter physics is that this analogy remains valid even when the electrons experience a static disorder potential, as in a resistive metal (*1*). Theoretical treatments of PCs in resistive metal rings have been developed over a number of decades [see (*1*, *2*) and references therein]. Calculations that take into account the electrons' inevitable coupling to the static disorder potential and a fluctuating thermal bath predict several general features. A micrometer-diameter ring will support a PC of $I \sim 1$ nA at temperatures $T \lesssim 1$ K. A magnetic flux Φ threading the ring will break time-reversal symmetry, allowing the PC to flow in a particular direction around the ring. Furthermore, the Aharonov-Bohm effect will require I to be periodic in Φ with period $\Phi_0 = h/e$, thereby providing a clear-cut experimental signature of the PC.

These predictions have attracted considerable interest, but measuring the PC is challenging for a number of reasons. For example, the PC flows only within the ring and so cannot be measured with a conventional ammeter. Experiments to date (*2*, *3*) have mostly used superconducting quantum interference devices (SQUIDs) to infer the PC from the magnetic field it produces. Interpretation of these measurements has been complicated by the SQUID's low signal-to-noise ratio (SNR) and the uncontrolled back action of the SQUID's ac Josephson oscillations, which may drive nonequilibrium currents in the rings. In addition, SQUIDs perform optimally in low magnetic fields; this limits the maximum Φ that can be applied to the rings, allowing observation of only a few oscillations of $I(\Phi)$ and complicating the subtraction of background signals unrelated to the PC.

Experiments to date have produced a number of confusing results in apparent contradiction with theory and even among the experiments themselves (*2*, *3*). These conflicts have remained without a clear resolution for nearly 20 years, suggesting that our understanding of how to measure and/or calculate the ground-state properties of as simple a system as an isolated metal ring may be incomplete.

More recent theoretical work has predicted that the PC is highly sensitive to a variety of subtle effects, including electron-electron interactions (*4*–*7*), the ring's coupling to its electromagnetic environment (*8*), and trace magnetic impurities within the ring (*9*). These theories have not explained all of the experimental results to date, but they do indicate that accurate measurements of the PC would be able to address a number of interesting questions in many-body condensed-matter physics (in addition to resolving the long-standing controversy described above).

We measured the PC in resistive metal rings using a micromechanical detector with orders of magnitude greater sensitivity and lower back-action than SQUID-based detectors. Our approach allows us to measure the PC in a single ring and arrays of rings as a function of ring size, temperature, and the magnitude and orientation of the magnetic field over a much broader range than has been possible previously. Quantitative agreement is found between these measurements and calculations based on a model of diffusive, non-interacting electrons. This agreement is supported by independent measurements of the rings' electrical properties.

Figure 1, A to C, shows single-crystal Si cantilevers with integrated Al rings [their fabrication is described elsewhere (*10*)]. All the PC measurements were made in magnetic fields well above the critical field of Al, ensuring that the rings were in their normal (rather than superconducting) state. The parameters of the four ring samples measured are given in Table 1.

In the presence of a magnetic field $\vec{B}$, each ring's current I produces a torque on the cantilever $\vec{\tau} = \vec{\mu} \times \vec{B}$ as well as a shift $\delta\nu$ in the cantilever's resonant frequency ν. Here $\vec{\mu} = \pi r^2 I \hat{n}$ is the magnetic moment of the PC, r is the ring radius, and $\hat{n}$ is the unit vector normal to the ring. We infer $I(B)$ from measurements of $\delta\nu(B)$; the conversion between $\delta\nu(B)$ and $I(B)$ is described in the supporting online material (SOM) text.

To monitor ν, we drive the cantilever in a phase-locked loop. The cantilever is driven via a piezoelectric element, and the cantilever's displacement is monitored by a fiber-optic interferometer (*11*). The cantilever's thermally limited force sensitivity is ~2.9 aN/Hz$^{1/2}$ at $T = 300$ mK, corresponding to a magnetic moment sensitivity of ~11 μ_B/Hz$^{1/2}$ and a current sensitivity of ~20 pA/Hz$^{1/2}$ for a ring with $r = 400$ nm at $B = 8$ T. By comparison, SQUID magnetometers achieve a current sensitivity $\gtrsim 5$ nA/Hz$^{1/2}$ for a similar ring (*12*–*14*). The noise temperature of the cantilever and the electron temperature of a metal sample at the end of a cantilever both equilibrate with the fridge temperature for the conditions we used (*11*).

The frequency shift of a cantilever containing an array of $N = 1680$ lithographically identical rings with $r = 308$ nm at $T = 323$ mK is shown (Fig. 1D) as a function of B. Oscillations with a period ≈20 mT, corresponding to a flux h/e through each ring, are visible in the raw data. Depending on r and θ (the angle between $\vec{B}$ and the plane of

---

[1] Department of Physics, Yale University, New Haven, CT 06520, USA. [2] Institut für Theoretische Physik, Freie Universität Berlin, Fachbereich Physik, 14195 Berlin, Germany. [3] Department of Applied Physics, Yale University, New Haven, CT 06520, USA.

EXTENDED PDF FORMAT
SPONSORED BY

Sample-Size Antibodies
Now Available
Learn More
R&D SYSTEMS
a biotechne brand
www.rndsystems.com

Repetitive Readout of a Single Electronic Spin via Quantum Logic with Nuclear Spin Ancillae

L. Jiang *et al.*

Science **326**, 267 (2009);
DOI: 10.1126/science.1176496

This copy is for your personal, non-commercial use only.

If you wish to distribute this article to others, you can order high-quality copies for your colleagues, clients, or customers by clicking here.

Permission to republish or repurpose articles or portions of articles can be obtained by following the guidelines here.

The following resources related to this article are available online at www.sciencemag.org (this information is current as of February 26, 2016):

Updated information and services, including high-resolution figures, can be found in the online version of this article at:
/content/326/5950/267.full.html

Supporting Online Material can be found at:
/content/suppl/2009/09/10/1176496.DC1.html

This article **cites 30 articles**, 4 of which can be accessed free:
/content/326/5950/267.full.html#ref-list-1

This article has been **cited by** 4 article(s) on the ISI Web of Science

This article has been **cited by** 10 articles hosted by HighWire Press; see:
/content/326/5950/267.full.html#related-urls

This article appears in the following **subject collections:**
Physics
/cgi/collection/physics

Downloaded from on February 26, 2016

Science (print ISSN 0036-8075; online ISSN 1095-9203) is published weekly, except the last week in December, by the American Association for the Advancement of Science, 1200 New York Avenue NW, Washington, DC 20005. Copyright 2009 by the American Association for the Advancement of Science; all rights reserved. The title *Science* is a registered trademark of AAAS.